6.- Theoretical models for corona and solar wind (kinetic models)

1. Introduction

The first evaporative or exospheric model for the solar wind was proposed by Chamberlain in 1960. On the analogy of the escape of neutral particles from a planetary exosphere, Chamberlain suggested that the radial expansion of the solar corona results from the thermal evaporation of the hot coronal protons. Assuming a Pannekoek-Rosseland electric potential distribution in the collisionfree exosphere (located above 2.5 solar radii) Chamberlain calculated a solar wind flow speed of about 20 km sec^{-1} at 1 A.U.

Since Parker's hydrodynamic calculations predicted a highly supersonic flow speed a controversy started between Parker and Chamberlain. Finally direct observations of the solar wind showed the existence of a

continuous supersonic plasma flow and the exospheric description of the solar wind was considered as an academic solution without any interest for the solar corona.

Later on Jensen (1963) and Brandt and Cassinelli (1966) proposed more elaborated exospheric models. They still used the Pannekoek-Rosseland field (Pannekoek, 1922; Rosseland, 1924). It was only at the beginning of this decade that the validity of the Pannekoek-Rosseland field in the ion-exosphere was questioned. The Pannekoek-Rosseland field which prevents charge separation in a collision dominated plasma under hydrostatic equilibrium conditions, cannot be the **true** electric field in the exosphere where the **gravitational** charge separation becomes less important than the charge separation of thermal origin.

The Pannekoek-Rosseland field decelerates the electrons and accelerates the protons **in** such a way that the combined gravitational and electric forces on electrons and protons become equal. Therefore, this field leads to equal densities of electrons and protons. The flux of the electrons however would be $(m_p/m_e)^{1/2} \approx 43$ times larger than the escape flux of the protons. Since this would cause a continuous charge deposition on the sun the **true** electric field must be larger to decelerate the electrons and to accelerate the protons more strongly than the **Pannekoek-Rosseland field does. This electric field must be determined in a** self consistent way **so** that the quasi-neutrality condition $n_e(r) = n_p(r)$ and the zero-current condition $F_e(r) = F_p(r)$ is satisfied in the exosphere (F_e : electron flux; F_p : proton flux). **Figures 1 and 2 illustrate the** difference between a self consistent calculated electric field **and potential,** and the Pannekoek-Rosseland field **and potential.**

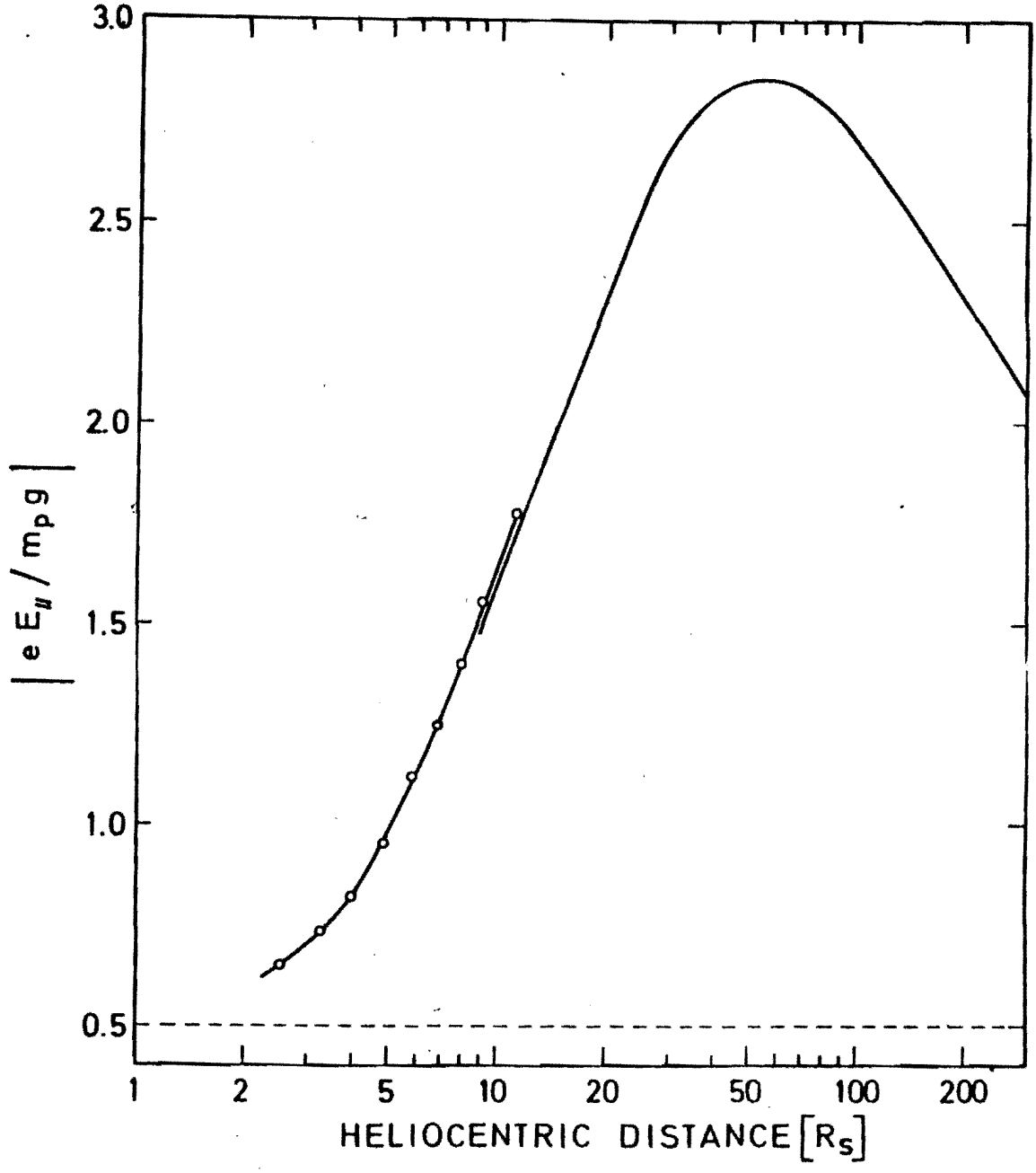

Fig. 1.- The ratio of the parallel electric force to the gravitational force acting on a proton in the solar wind. The solid line corresponds to the kinetic model 1 of Lemaire and Scherer [1972c]. The dots correspond to empirical values deduced from Pottasch's [1960] observed coronal density distribution. The dashed line corresponds to Pannekoek-Rosseland's electrostatic potential distribution.

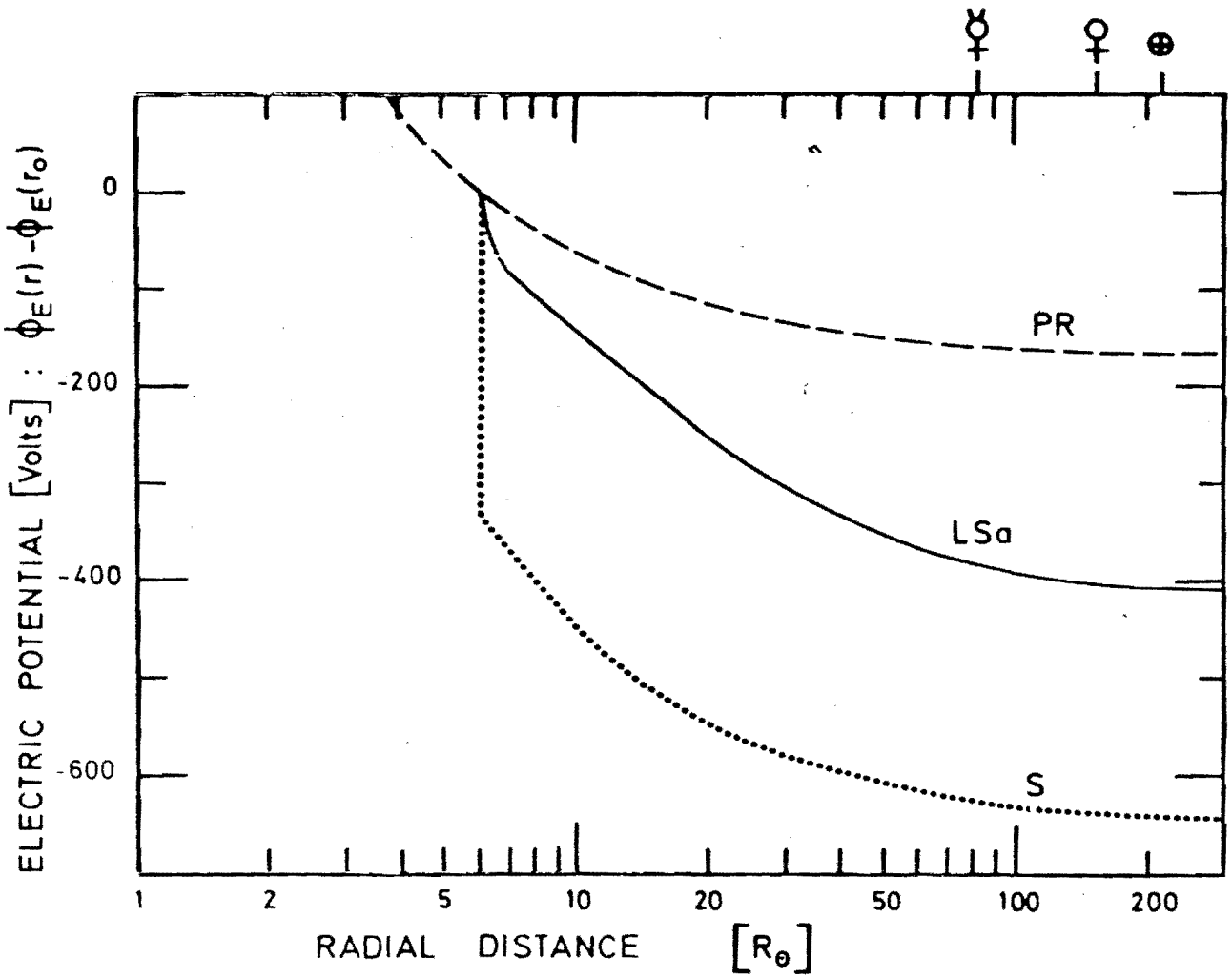

Fig. 2.- The electric potential in some exospheric models of the solar corona. The dashed line (PR) illustrates the Pannekoek Rosseland's distribution ; the dotted curve (S) gives Sen's exospheric model for a baropause $r_o = 6.05\ R_\odot$ and a temperature $T(r_o) = 10^6\ ^\circ K$; the solid line (LSa) corresponds with the kinetic models of Lemaire and Scherer for the same baropause conditions.

2. DESCRIPTION OF A KINETIC MODEL

2.1. Assumptions

- Guiding center approximation
- Non-rotating sun
- Spherical symmetric outflow
- The collisionfree exosphere is separated from the collision dominated region by a **sharply** defined surface : the exobase.
- Radial magnetic field $B(\vec{r}) \sim r^{-2}$

This last assumption is not restrictive, the exospheric model remains valid for the more general case in which the magnetic field strength is a monotonic decreasing function along a field line. For the sun however, the magnetic field lines of the spiral field model are radial if solar rotation is neglected.

2.2. Single-particle Trajectories

According to the single-particle picture of a plasma there exist two invariants of the motion :

- the total energy :

$$\frac{1}{2} m v^2(\vec{r}) + m \phi_g(\vec{r}) + Ze \varphi(\vec{r}) = \text{constant} \qquad (1)$$

$$\phi_g(\vec{r}) = - G \frac{M_\odot}{r}$$

$$Z_e = - 1$$

$$Z_p = + 1$$

$\varphi(\vec{r})$ is the electrostatic potential due to a very small charge separation of thermal origin. Because the flow speed of the solar wind is substantially below the electron thermal velocity, the electrostatic potential will reflect most of the electrons and $\varphi(r)$ will be a monotonic decreasing function of radial distance. The electric field, $\vec{E} = -\vec{\nabla}\varphi$, which is directed outwards, accelerates the protons and decelerates the electrons.

- the magnetic moment or 1st adiabatic invariant

$$\frac{m\, v_{\perp}^2(\vec{r})}{2\, B(\vec{r})} = \text{const.}$$

or

$$\frac{v^2(\vec{r})\, \sin^2 \theta(\vec{r})}{B(\vec{r})} = \text{const} \qquad (2)$$

where $\theta(r)$ is the pitch angle; i.e. the angle between the velocity vector and the magnetic field. Equations (1) and (2) define unambiguously the single particle trajectories in the collisionfree exosphere.

Those trajectories can be classified into four classes :

1. The ballistic particles emerge from the exobase but are reflected because they have not enough kinetic energy to escape ;
2. The escaping particles emerge from the exobase and are lost in the interplanetary space;
3. The trapped particles have a periodically motion between two mirror points in the exosphere. The lower mirror point is a magnetic mirror point; the upper reflection is due to the fact that the kinetic energy of those particles is not large enough to pass the potential barrier.

4. The incoming particles : these particles come from infinity and are reflected in the exosphere or they reach the exobase and are lost in the collision dominated region. For the solar wind this class of particles is almost empty.

To determine the different regions in phase space corresponding to those classes we apply (1) and (2) between r_o and $r > r_o$. Hence we obtain :

$$(1) \rightarrow \quad v^2(r_o) = v^2(r) + [\ \psi(r) - \psi(r_o)]$$

$$\text{with} \quad \psi(r) = 2\left[\phi_g(r) + \frac{Ze}{m}\ \varphi(r)\right]$$

$$(2) \rightarrow \quad \sin^2\theta(r_o) = G(r_o,r)\ \sin^2\theta(r)$$

$$\text{with} \quad G(r_o,r) = \frac{B(r_o)}{B(r)}\ \frac{v^2(r)}{v^2(r_o)} \quad ; \quad \frac{B(r_o)}{B(r)} > 1 \quad \text{for } r_o < r$$

If we assume that the potential energy is a monotonic function along a magnetic field line we have to consider two cases.

1st. $\psi(r)$ is a monotonic decreasing function

This will be the case for the protons and is illustrated in Fig. 3a. All particles at the exobase with a velocity vector directed outwardly are accelerated continuously and will escape. There will be no ballistic nor trapped particles.

2nd. $\psi(r)$ is a monotonic increasing function

This will be the case for the electrons and is illustrated in Fig. 3b. Escaping particles have to overcome a potential barrier and

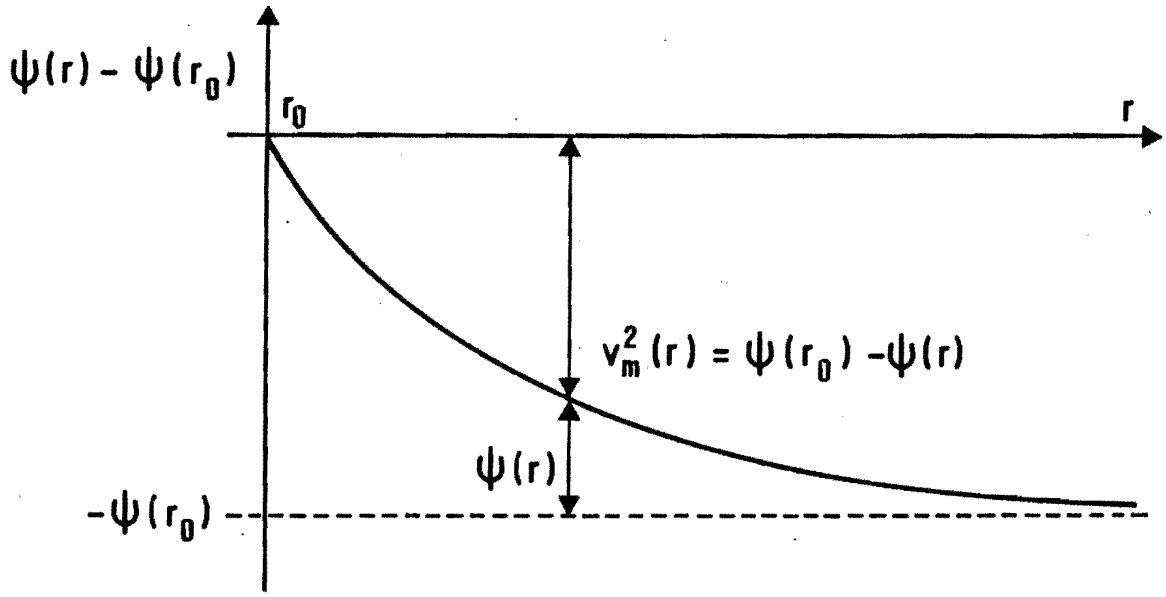
ψ(r) - ψ(r0)
r0
r
v²m(r) = ψ(r0) -ψ(r)
ψ(r)
-ψ(r0)

Fig. 3a

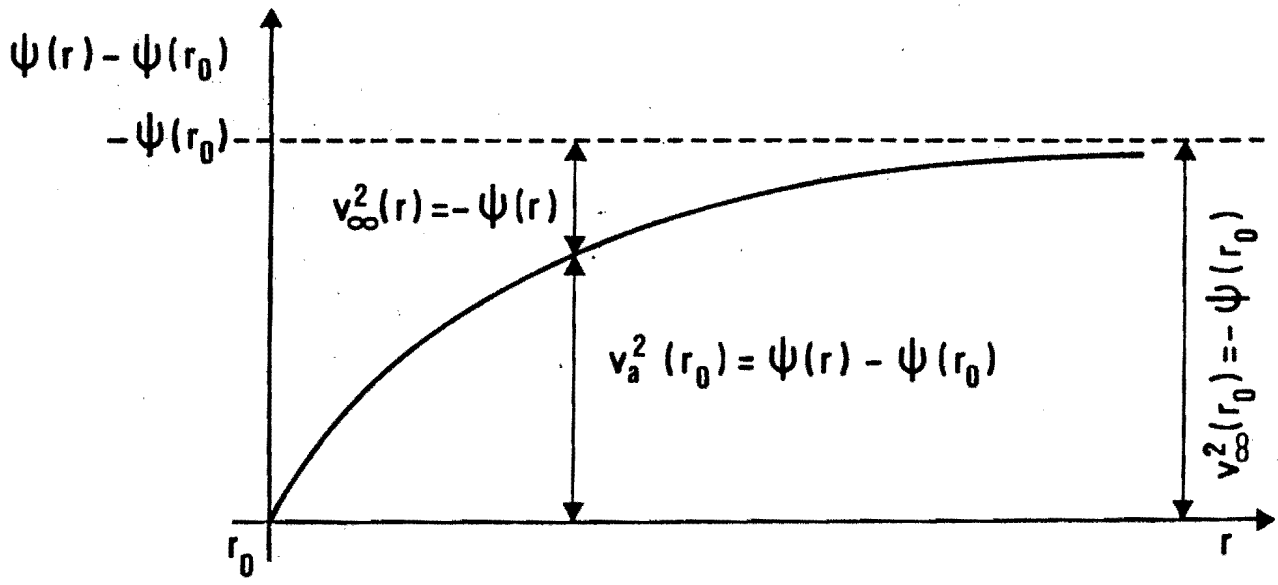
ψ(r) - ψ(r0)
-ψ(r0)
v²∞(r) =- ψ(r)
v²a (r0) = ψ(r) - ψ(r0)
v²∞(r0) =- ψ(r0)
r0
r

Fig. 3b

therefore their velocity at the exobase must be larger than the minimum escape velocity $v_\infty(r) = [-\psi(r)]^{1/2}$.

Particles with velocities $v(r_o) < v_a(r_o) \equiv [\psi(r) - \psi(r_o)]^{1/2}$ will never reach the level r because they have not enough kinetic energy.

Particles with velocities $v_a(r_o) < v(r_o) < v_b(r_o) \equiv v_a(r_o)/[1 - B(r)/B(r_o)]$ and pitch angles $o < \theta(r_o) < \theta_m(r_o) \equiv \arcsin\{[G(r_o,r)]^{1/2}\}$ will reach r. If they have a pitch angle $\theta_m(r_o) < \theta(r_o) < \frac{\pi}{2} - \theta_m(r_o)$, however, they will be reflected by a magnetic mirror point before reaching r.

Particles with velocities $v(r_o) > v_b(r_o)$ will always reach level r where their velocities and pitch angles satisfy the following inequalities

$$v(r) > v_b(r) \equiv \frac{B(r)}{B(r_o)}\, v_b(r_o)$$

$$o < \theta(r) < \theta_m(r) \equiv \arcsin\{[G(r_o,r)]^{-1/2}\}$$

In this case there are also trapped particles. All possible classes of particles at the level r are illustrated in Fig. 4.

2.3. The velocity distribution

The velocity distribution is a solution of the collisionless Boltzmann equation or Vlasov's equation which states that the distribution function $f(\vec{r}, \vec{v})$ is constant along phase space trajectories. The phase space trajectories are characterized by constants of motion. Therefore any function of the constants of motion is a solution of Vlasov's equation.

Owing to the truncation procedure that excludes the incomming particles it is obvious that the function $f[r_o, \vec{v}(r_o)]$ adopted in kinetic calculations

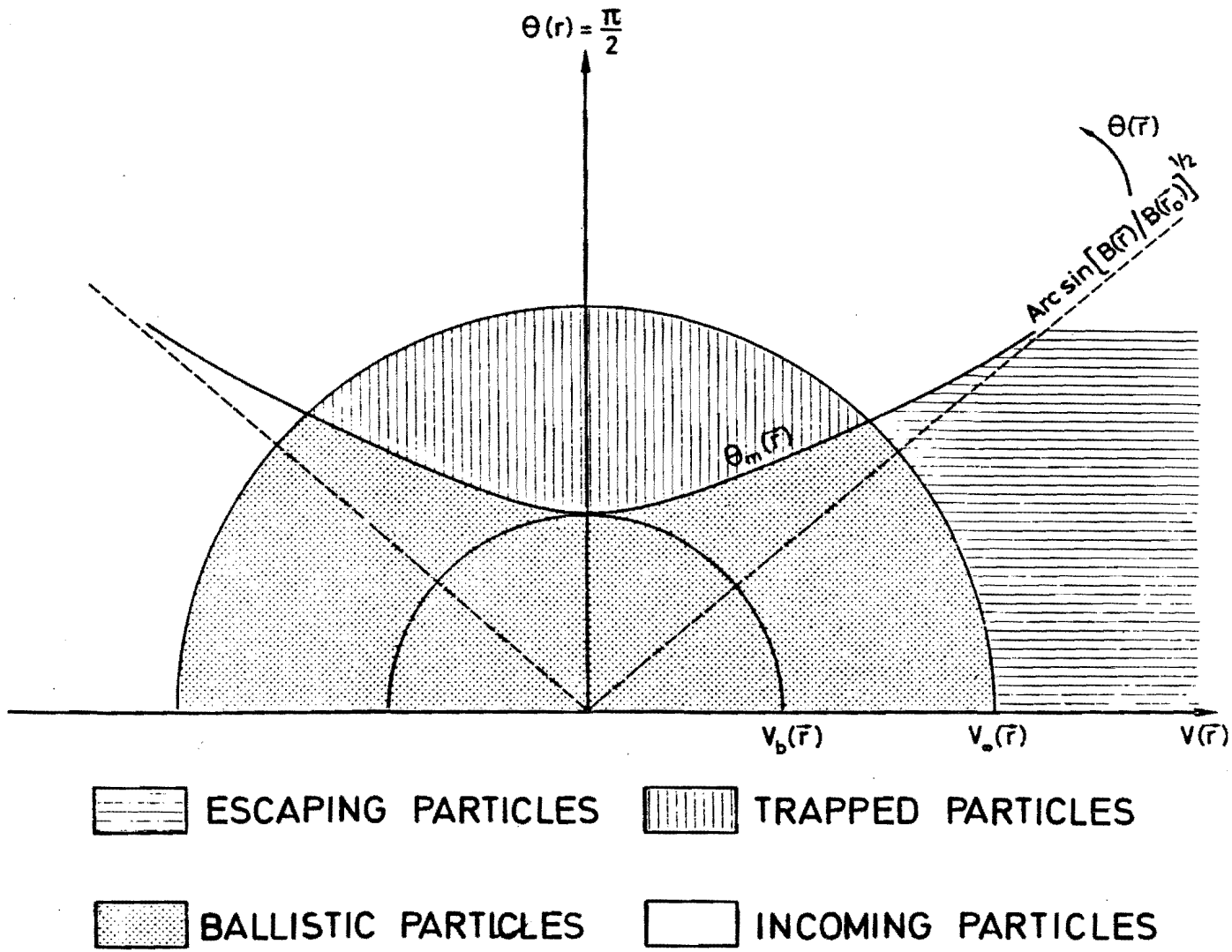
$\theta(r) = \frac{\pi}{2}$
$\theta(\bar{r})$
$\text{Arc sin}\left[B(\bar{r})/B(\bar{r}_o)\right]^{1/2}$
$\theta_m(\bar{r})$
$V_b(\bar{r})$
$V_o(\bar{r})$
$V(\bar{r})$
ESCAPING PARTICLES
TRAPPED PARTICLES
BALLISTIC PARTICLES
INCOMING PARTICLES

Fig. 4.-

is not necessarily a realistic microscopic representation of the actual velocity distribution at the exobase. It is however always possible to build up a function $f[r_o, \vec{v}(r_o)]$ so that the s first moments coincide with the s corresponding moments of the actual velocity distribution at the exobase.

For example a linear combination of truncated Maxwellians

$$f[r_o, \vec{v}(r_o)] = \sum_j c_j e^{-\beta_j v^2(r_o)}$$

is appropriate since kinetic models usually have been developed for Maxwellian distribution functions. The parameters c_j and β_j can be determined so that the density, the flux, the temperature, the anisotropy or any higher order momentum coincide with the actual values at the exobase. This method avoids zero order discontinuities (jumps) at the exobase, but first order discontinuities (gradient-discontinuities) can not be avoided because of the sharp transition between the collision dominated and collisionfree regions.

In what follows we will assume a Pseudo-Maxwell-Boltzmann distribution

$$f[r_o, \vec{v}(r_o)] = N \left(\frac{m}{2\pi kT}\right)^{3/2} e^{-\frac{m}{2kT} v^2(r_o)}$$

were the incoming particles are missing. This is illustrated in Fig. 5. Therefore

$$n(r_o) \neq N \text{ and } T(r_o) \neq T$$

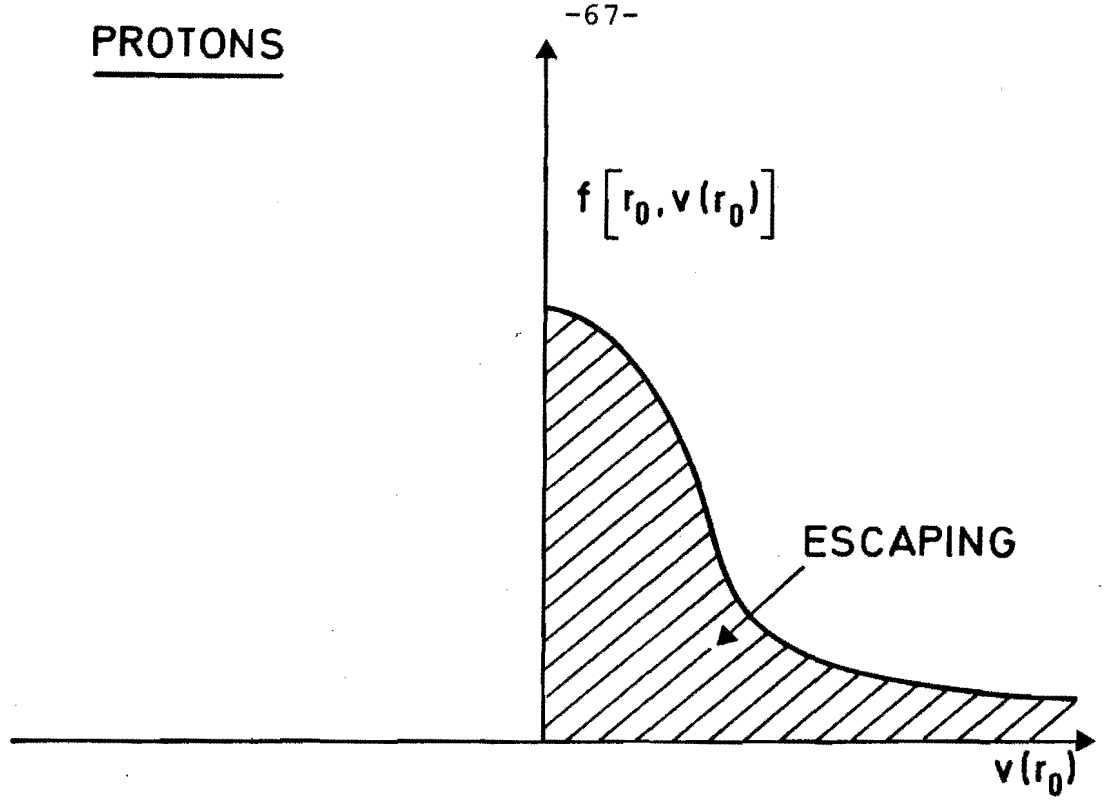
PROTONS
f [r0, v(r0)]
ESCAPING
v(r0)

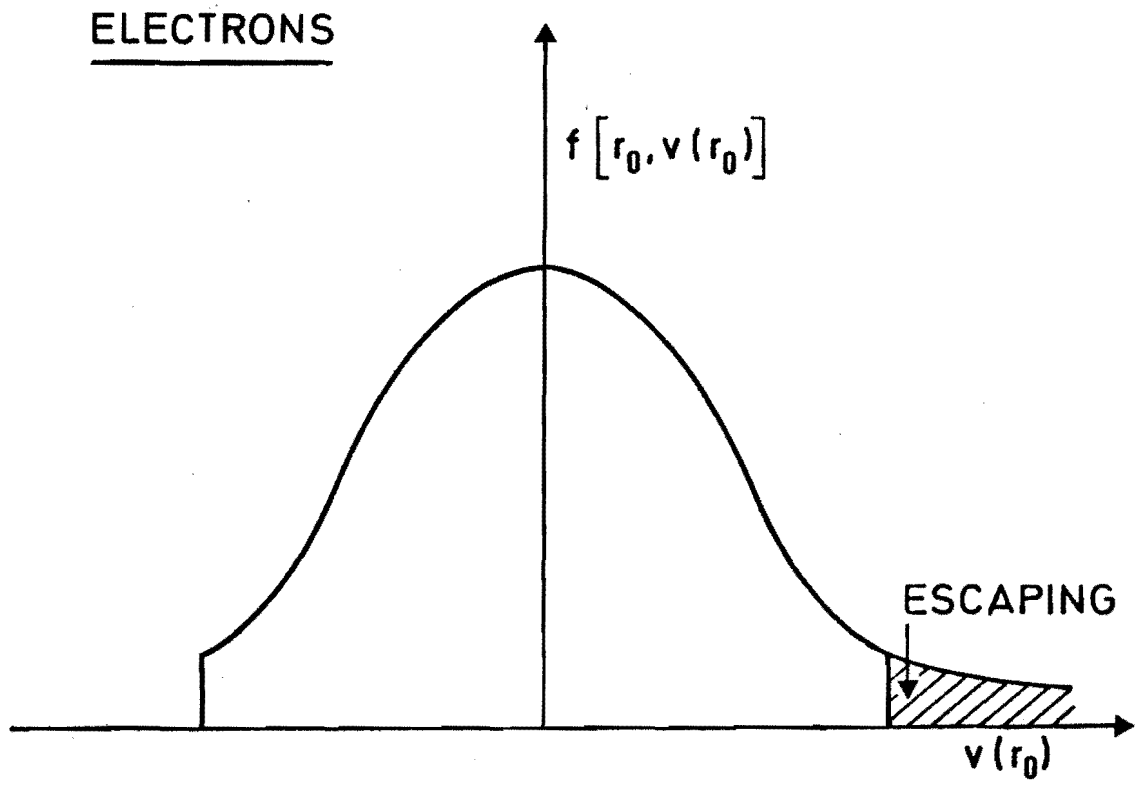
ELECTRONS
f [r0, v(r0)]
ESCAPING
v(r0)

Fig. 5.-

The velocity distribution in the collisionfree region ($r > r_o$) follows from Liouville's theorem :

$$f[r, \vec{v}(r)] = N(m/2\pi kT)^{3/2} \; e^{-Q} \exp\left[- \frac{m}{2kT} \; v^2(r) \right]$$

with $$Q = \frac{m}{2kT} \; [\psi(r) - \psi(\vec{r}_o)]$$

2.4. Moments of the distribution function

- particle density : $$n(r) = \int f(r, \vec{v}) \, d^3v$$

- particle flux : $$F(r) = \int v_{\parallel} f(r, \vec{v}) \, d^3v$$

- momentum fluxes : $$P_{\parallel}(r) = m \int v_{\parallel}^2 \, f(r, \vec{v}) \, d^3v$$

$$P_{\perp}(r) = \frac{1}{2} m \int v_{\perp}^2 \, f(r, \vec{v}) \, d^3v$$

- energy flux : $$\epsilon(r) = \frac{1}{2} m \int v^2 \, v_{\parallel} f(r, \vec{v}) \, d^3v$$

- flow speed : $$w(r) = F(r)/n(r)$$

- Temperatures : $$T_{\perp}(r) = P_{\perp}(r)/k \; n(r)$$

$$T_{\parallel}(r) = \frac{P_{\parallel}(r) - m \, w(r) \, F(r)}{k \; n(r)}$$

$$T(r) = \frac{1}{3} [T_{\parallel}(r) + 2 \, T_{\perp}(r)]$$

- Anisotropy : $$a(r) = T_{\parallel}(r)/T_{\perp}(r)$$

- Conduction flux : $$C(r) = \frac{1}{2} m \int (\vec{v} - \vec{w})^2 \, (v_{\parallel} - w) \, f(r, \vec{v}) \, d^3v$$

$$= \epsilon(r) + w(r) \left[m \, w(r) \, F(r) - \frac{3}{2} P_{\parallel}(r) - P_{\perp}(r) \right]$$

2.5. Calculation of the electrostatic potential

The explicit formula of the escape flux shows that the proton flux is independant of the electrostatic potential, whereas the electron flux depends only on the height of the potential barrier $[-\psi(r_o)]$, i.e. on $\varphi(r_o)$ and not on $\varphi(r)$. Therefore the zero-current condition $F_e(r) = F_p(r)$ can be used to calculate $-\psi_e(r_o)$ or $\varphi(r_o)$.

The local quasi-neutrality condition $n_e(r) = n_p(r)$ can then be used to calculate the electrostatic potential distribution, $\varphi(r)$, from which the electric field $E = -\frac{d\varphi(r)}{dr}$ can be deduced. Moreover we can also calculate the average temperatures and temperature anisotropies, the energy fluxes and conduction fluxes, etc..., since the self-consistent electrostatic potential distribution is known in the collisionfree exosphere.

3. APPLICATION TO QUIET SOLAR WIND CONDITIONS

To calculate a solar wind model by means of the previous exospheric approximation we first have to determine the exobase level. This is the surface where the mean free path l becomes equal to the density scale heigth H.

The proton mean free path is given by

$$l_p = 1.8 \times 10^5 \frac{T_p^2}{n_e \ln \Lambda_{pp}} \quad [\text{cm}]$$

where the Coulomb logarithm is practically constant and equal to 25 for the temperatures and densities considered.

The density distribution n_e can be deduced from observations of the solar corona (Pottasch, 1960) for $r < 20$ solar radii. Hence we can also calculate the scale height $H = \left(-\frac{d \ln n_e}{dr}\right)^{-1}$. These results are shown in Fig. 6, curve 1 for the density and curve 2 for the scale height.

For a given proton temperature T_p; the proton exobase follows from the condition $l_p(r_o) = H(r_o)$; or inversely if the exobase level is known we can determine the proton temperature by means of

$$\log T_p(r_o) = \frac{1}{2} \log n_e(r_o) + \frac{1}{2} \log H(r_o) + 0.57$$

where n_e is given in cm^{-3} and H in km. Curve 3 in Fig. 6 shows $T_p(r_o)$ obtained from Pottasch's electron density distribution.

The mean free path for the electrons is given by

$$l_e = 0.416 \, (T_e/T_p)^2 \, l_p$$

and the electron exobase follows from the condition $l_e(r_o) = H(r_o)$.

In what follows we will assume that the electron exobase coïncides with the proton exobase. This yields the constraint $l_e = l_p$ or

$$T_p(r_o) = 0.645 \, T_e(r_o) \, .$$

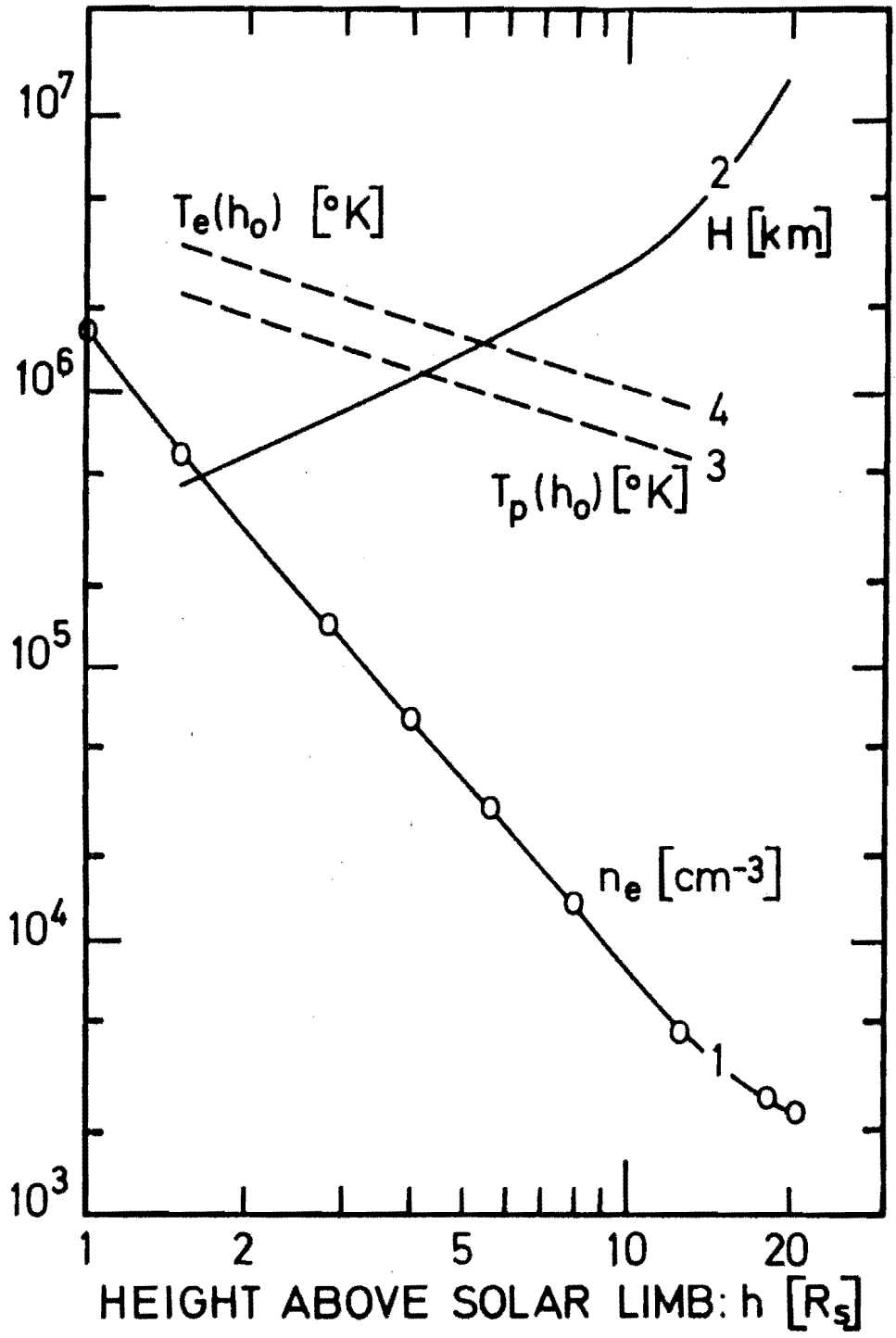

Fig. 6.- Curve 1 shows the equatorial electron density distribution (cm^{-3}) in the solar corona observed during an eclipse near minimum in the sunspot cycle as reported by Pottasch [1960] ; Curve 2 gives the corresponding density scale height, H, in km ; Curves 3 and 4 illustrate respectively the proton and electron temperatures at the exobase as a function of the exobase altitude h_o expressed in solar radii.

The electron temperatures corresponding to Pottasch's density distribution are shown in Fig. 6, curve 4.

Fig. 6 can be used to determine the boundary conditions for the exospheric solar wind models. Indeed if we choose an electron temperature at the exobase we can determine the exobase level r_o by curve 4; the density $n(r_o)$ by curve 1 and the proton temperature by curve 3.

In Fig. 7 and 8 we plotted respectively the solar wind flow speed and density at 1 AU and the average electron and proton temperature at 1 AU calculated for different electron temperatures at the exobase. From the results we conclude that there exists a positive correlation between the flow speed and the proton temperature at 1 AU whereas the electron temperature at 1 AU is nearly independent from the bulk velocity at 1 AU. This positive correlation which is also supported by solar wind measurements is illustrated in Fig. 9.

Since the proton velocity distribution at the exobase can be highly asymmetric, we also considered kinetic models in which the proton velocity distribution at the exobase is given by

$$f\,[\,r_o,\ v(r_o)] = N(m/2\pi kT)^{3/2} \exp\left[- \frac{m}{2kT} (\vec{v} - \vec{u})^2 \right]$$

where $\vec{u}$ is a velocity vector parallel to the magnetic field. Since the incoming particles are missing u is not the flow speed at the exobase but a parameter which can be chosen in order to obtain a given flux or bulk velocity at r_o.

Fig. 10 and 11 illustrate the influence of u_p on the solar wind flow speed, density and average electron and proton temperature at 1 AU.

Finally, in Table 1 we compare the results from a calculated solar wind model with the observations reported by Hundhausen [1968, 1970, 1972a,b].

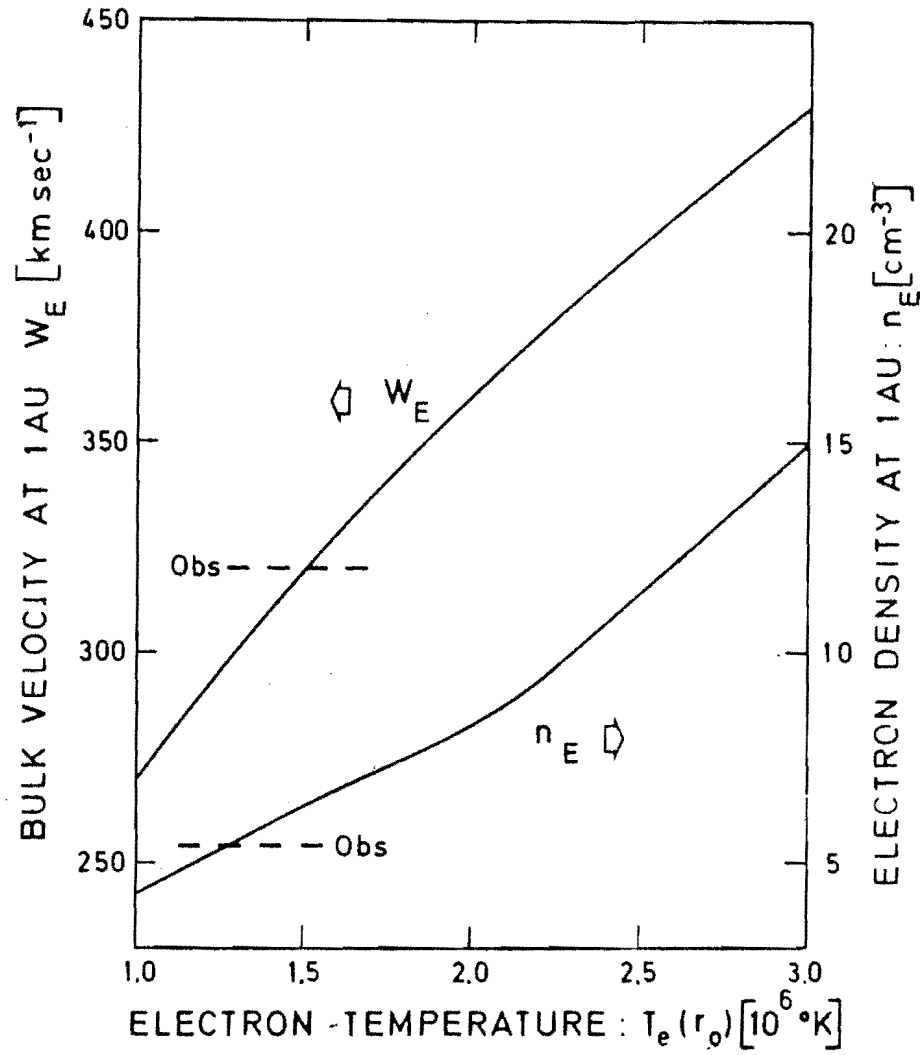

Fig. 7.- The bulk velocity W_E (left hand scale), and the electron density n_E (right hand scale) at 1AU for $U_p = U_e = 0$ versus the electron temperature at the baropause. The observed (Obs) quiet solar wind flow speed and density are also plotted.

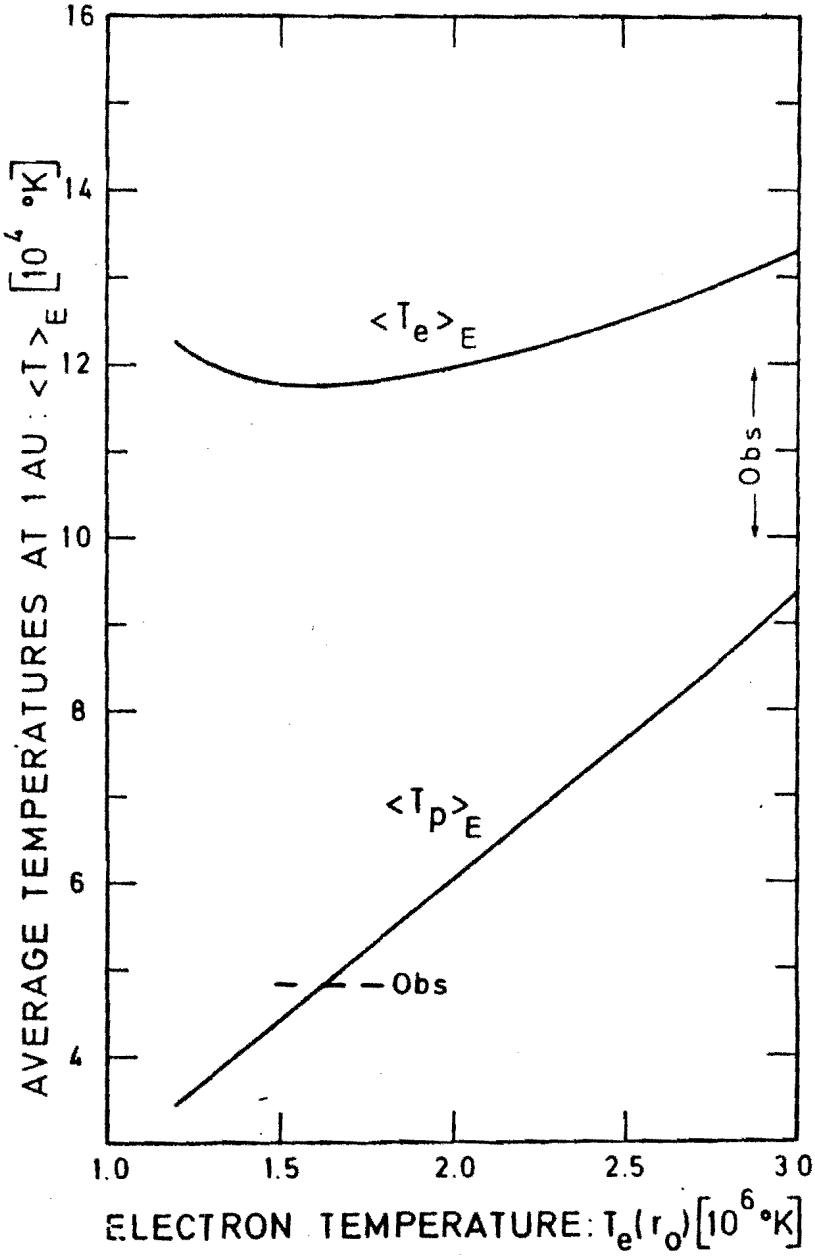

Fig. 8.- The average electron and proton temperatures at 1 AU and for $U_p = U_e = 0$, versus the electron temperature at the baropause. The observed (Obs) quiet solar wind values are also plotted.

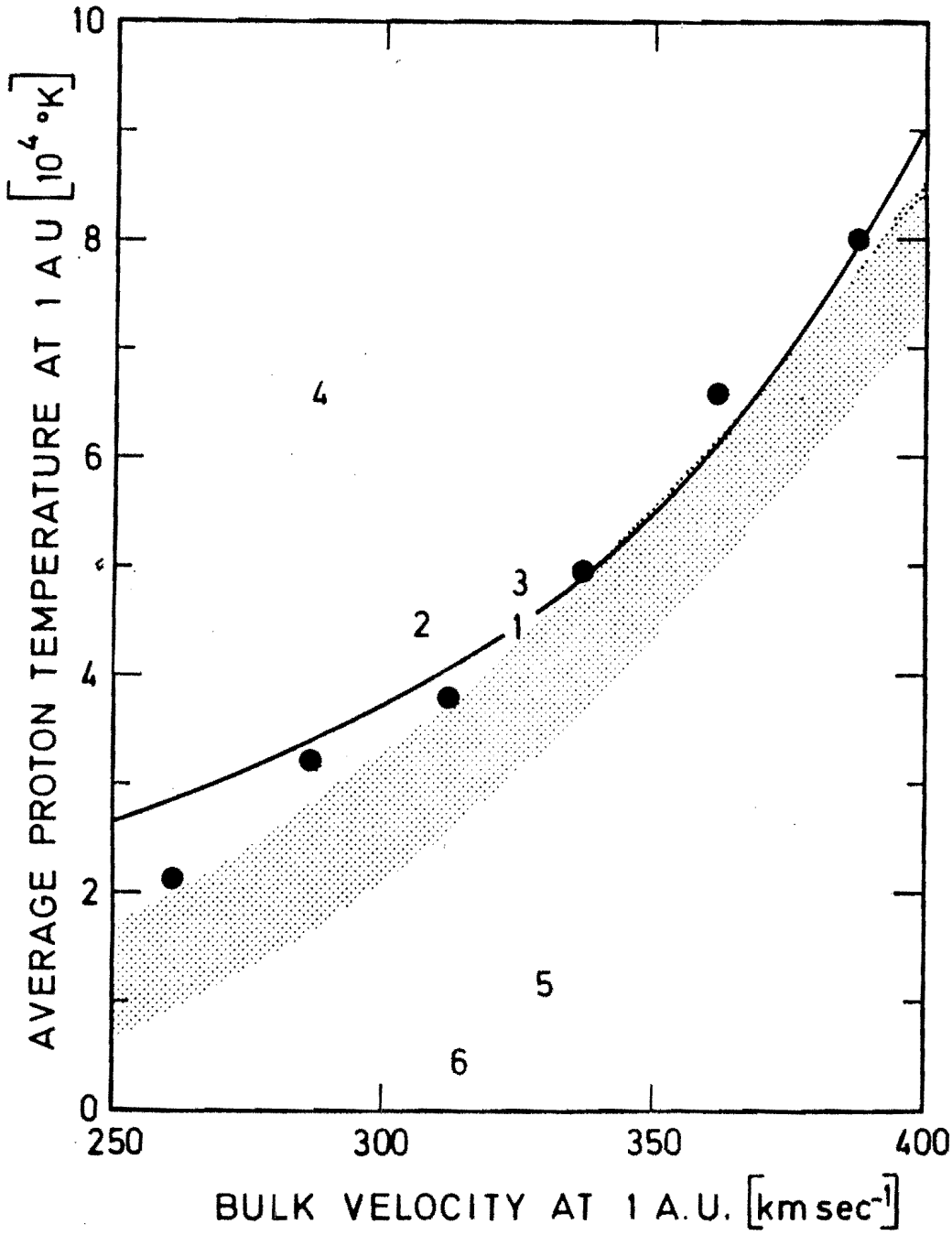

Fig. 9.- Correlation between the solar wind velocities and average proton temperatures at 1 AU. The solid dots correspond to Vela 3 measurements [Hundhausen *et al.*, 1970]. The shaded area corresponds to Explorer 34 data illustrated by the relation : $\langle T_p \rangle_E^{1/2} = (0.036 \pm 0.003) w_E \cdot (5.54 \pm 1.50)$ proposed by Burlaga and Ogilvie [1970]. Point 1 gives the quiet solar wind condition [Hundhausen, 1972a] ; Points 2 to 6 give the results obtained from the kinetic and semi-kinetic models reported in Table II from the second to the sixth line. The solid line shows the relationship deduced by Lemaire [1971] and discussed in the text.

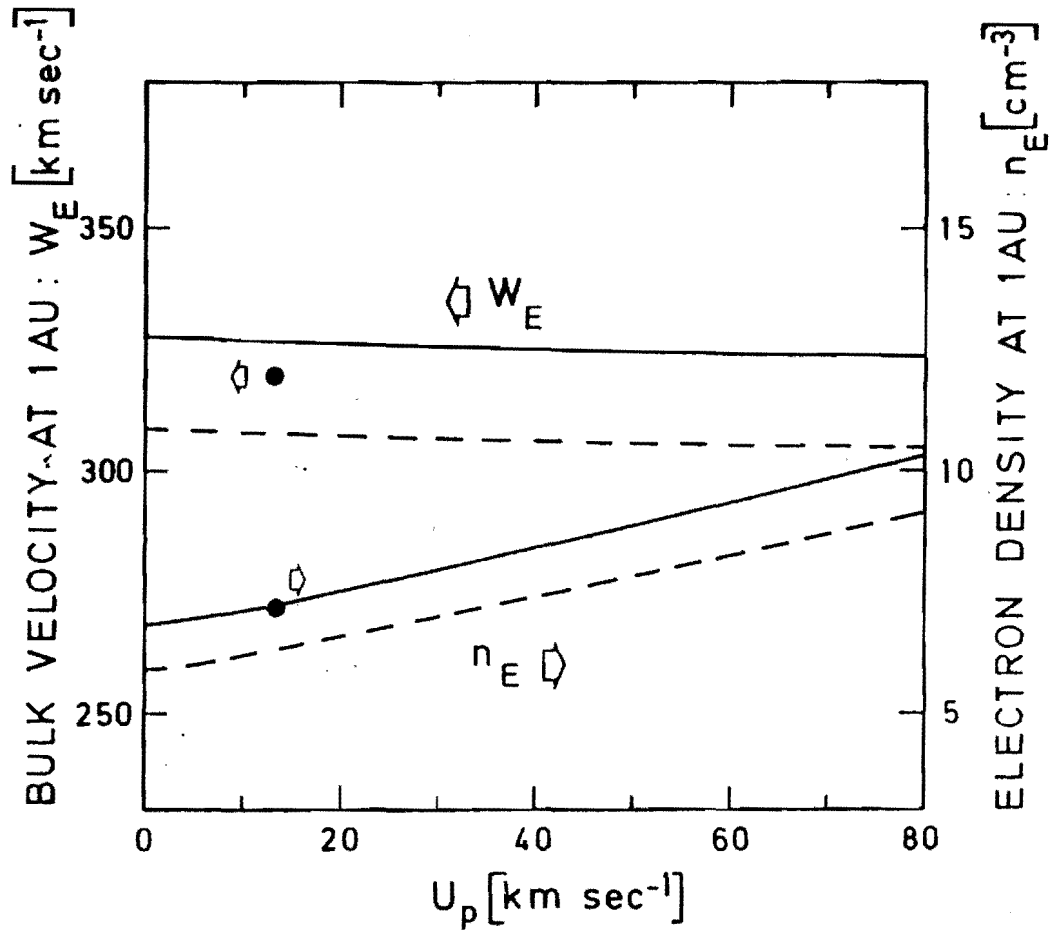

Fig. 10.- The bulk velocity W_e (left hand scale), and the electron density n_E (right hand scale) at 1 AU, versus U_p. The dashed and solid lines correspond to an electron temperature at the baropause of respectively 1.4×10^6 °K and 1.6×10^6 °K. The dots illustrate the model LSb which corresponds with the baropause conditions $r_o = 6.6\ R_\odot$, $T_e(r_o) = 1.52 \times 10^6$ °K, $T_p(r_o) = 0.984 \times 10^6$ °K, $U_e = 0$, $U_p = 14$ km sec^{-1}, and $n_e(r_o) = 3.1 \times 10^4$ cm^{-3}.

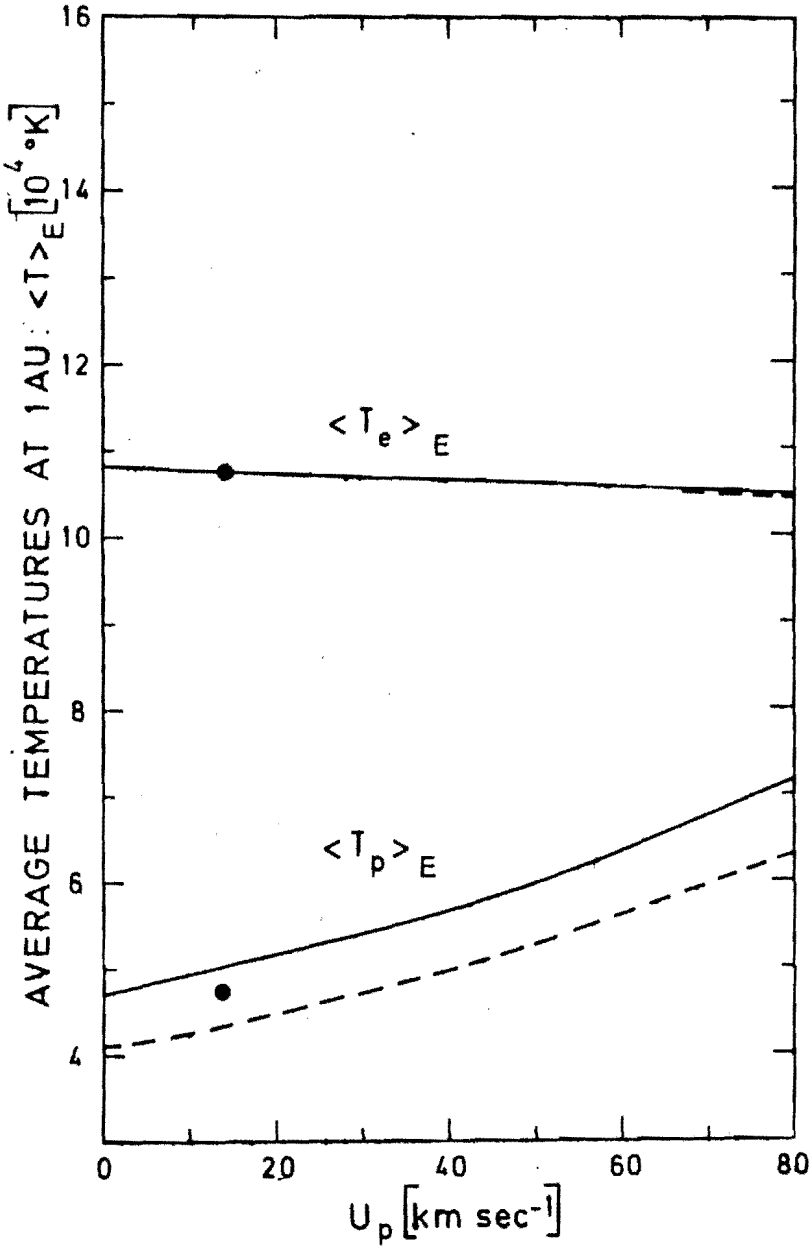

Fig. 11.- The average electron and proton temperatures at 1 AU, versus U_p. The dashed and the solid lines correspond respectively to an electron temperature at the baropause of 1.4×10^6 °K and 1.6×10^6 °K. The dots illustrate the model LSb which corresponds with the baropause conditions $r_o = 6.6\ R_.$, $T_e(r_o) = 1.52 \times 10^6$ °K, $T_p(r_o) = 0.984 \times 10^6$ °K, $U_e = 0$, $U_p = 14$ km sec^{-1}, and $n_e(r_o) = 3.1 \times 10^4$ cm^{-3}.

TABLE I : Results at 1 AU for the solar wind model r_o = 6.6 solar radii, $T_e(r_o) = 1.52 \times 10^6$ K ; $T_p(r_o) = 0.934 \times 10^6$ K , $n(r_o) = 3.1 \times 10^4$ cm^{-3} ; $u_e = o$; $u_p = 14$ km sec^{-1}. The observations are reported by Hundhausen (1963, 1970, 1972a, b).

At 1 AU	Model	Observations
w [km sec^{-1}]	320	300 - 350
n [cm^{-3}]	7.2	8.7 $\pm$ 4.6
F [cm^{-2} sec^{-1}]	2.3×10^8	1.2×10^8 - 4.6×10^8
T_e [K]	11.7×10^4	$(14 \pm 5) \times 10^4$
T_p [K]	4.8×10^4	$(4.4 \pm 1.8) \times 10^4$
$(T_{//}/T_{\perp})_e$	3.05	1.1 - 1.2
$(T_{//}/T_{\perp})_p$	164	2 $\pm$ 1
ε_p [erg cm^{-2} sec^{-1}]	0.2	$\approx$ 0.24
C_e [erg cm^{-2} sec^{-1}]	5.1×10^{-2}	$O(10^{-2})$

Except for the temperature anisotropies the agreement is quite good. The smaller calculated temperature anisotropy for the electrons compared to the protons is a consequence of the large number of trapped electrons present at 1 AU. Since the calculated anisotropies are much larger than the observed ones it is suggested that some scattering mechanism must modify the pitch angle distribution between the exobase and 1 AU.

REFERENCES

BRANDT, J.C., and J.P. CASSINELLI, Interplanetary gas, 11, An exospheric model of the solar wind, Icarus, 5, 47-63, 1966.

BURLAGA, L.F., and K.W. OGILVIE, Heating of the solar wind, Astrophys. J., 159, 659-670, 1970.

CHAMBERLAIN, J.W., Interplanetary gas, 2, Expansion of a model solar corona, Astrophys. J., 131, 47-56, 1960.

HOLLWEG, J.V., Collisionless solar wind, 1, Constant electron temperature, J. Geophys. Res., 75, 2403-2418, 1970.

HOLLWEG, J.V., Collisionless solar wind, 2, Variable electron temperature, J. Geophys. Res., 76, 7491-7502, 1971.

HUNDHAUSEN, A.J., Direct observations of solar-wind particles, Space Sci. Rev., 8, 690-749, 1968.

HUNDHAUSEN, A.J., Composition and dynamics of the solar wind plasma, Rev. Geophys. Space Phys., 8, 729-811, 1970.

HUNDHAUSEN, A.J., Composition and dynamics of the solar wind plasma, in Solar-Terrestrial Physics/1970, part 2, edited by E.R. Dyer, pp. 1-31, D. Reidel, Dordrecht, Netherlands, 1972a.

HUNDHAUSEN, A.J., Coronal Expansion and Solar Wind, 238 pp., Springer, Berlin, 1972b.

HUNDHAUSEN, A.J., S.J. BAME, J.R. ASBRIDGE, and S.J. SYDORIAK, Solar wind proton properties : Vela 3 observations from July 1965 to June 1967, J. Geophys. Res., 75, 4643-4657, 1970.

JENSEN, E., Mass losses through evaporation from a completely ionized atmosphere with applications to the solar corona, Astrophys. Norv., 8, 99-126, 1963.

JOCKERS, K., Solar wind models based on exospheric theory, Astron. Astrophys., 6, 219-239, 1970.

LEER, E., and T.E. HOLZER, Collisionless solar wind protons : A comparison of kinetic and hydrodynamic descriptions, J. Geophys. Res., 77, 4035-4051, 1972.

LEMAIRE, J., and M. SCHERER, Simple model for an ion-exosphere in an open magnetic field, Phys. Fluids, 14, 1683-1694, 1971a.

LEMAIRE, J., and M. SCHERER, Kinetic models of the solar wind, J. Geophys. Res., 76, 7479-7490, 1971b.

LEMAIRE, J., and M. SCHERER, Ion-exosphere with asymmetric velocity distribution, Phys. Fluids, 15, 760-766, 1972a.

LEMAIRE, J., and M. SCHERER, Comportements asymptotiques d'un modèle cinétique du vent solaire, Bull. Cl. Sci. Acad. Roy. Belg., 58, 1112-1134, 1972b.

LEMAIRE, J., and M. SCHERER, Kinetic models of the solar and polar winds, Rev. Geophys. Space Phys., 11, 427-468, 1973.

PANNEKOEK, A., Ionization in stellar atmospheres, Bull. Astron. Inst. Neth., 1, 107-118, 1922.

POTTASCH, S.R., Use of the equation of hydrostatic equilibrium in determining the temperature distribution in the outer solar atmosphere, Astrophys. J., 131, 68-74, 1960.

ROSSELAND, S., Electrical state of a star, Mon. Notic. Roy. Astron. Soc., 84, 720-728, 1924.

SEN, H.K., The electric field in the solar coronal exosphere and the solar wind, J. Franklin Inst., 287, 451-456, 1969.